Phenomenological Study of Baryon-Resonance Production in Neutrino-Nucleon Scattering

Daniel Norman

Tufts University, Medford, MA 02155

May 3, 2016

Abstract

Neutrino-nucleon interactions are a subject of great interest in modern physics. Baryon resonance reactions, characterized by the creation of a short-lived particle at the interaction vertex, represent a significant contribution to the total cross section of neutrino-nucleon scattering. The $\Delta(1232)$ particles, which decay into nucleons and pions, are known examples of resonance particles that carry baryon number =1. Bubble chamber experiments suggest there may be other baryon-resonance states with masses greater then that of the Δ state. However, the presence of these higher mass resonance particles in neutrino-nucleon scattering is not established. The value of the axial vector mass of the resonance reaction is also not unknown. I reviewed several papers on Δ-resonance production phenomenology, and I used these papers to write a simulation of resonance production. In this Thesis I present the design of the simulation and results obtained with it. Experimental research groups use GENIE, a Monte Carlo program, to generate neutrino-nucleon interaction events. By comparing the results of my simulation to GENIE predictions, I obtain evidence for the existence of higher-mass baryon resonance states. I also present new constraints on the value of the axial vector mass for baryon-resonance reactions within the context of contemporary resonance production phenomenology.

1 Introduction

1.1 Charged-Current Baryon-Resonance Production

Single pion production via charged-current (CC) neutrino or anti-neutrino interactions on nuclear media has been investigated experimentally. Very often these reactions proceed by intermediate production of baryon-resonance states. For example, a neutrino (ν_μ) may react with a nucleon (N) to produce a muon (μ) and a Delta (Δ) resonance state:

$$\nu_\mu \mathrm{N} \rightarrow \mu^- + \Delta^{++,+} \rightarrow \mu^- \mathrm{N}\pi \tag{1}$$

$$\bar{\nu_\mu}\mathrm{N} \rightarrow \mu^+ + \Delta^{0,-} \rightarrow \mu^+\mathrm{N}\pi \tag{2}$$

The $\Delta(1232)$ then decays via the strong nuclear force into a nucleon and a pion (π). The mean lifetime of a Δ particle is on the order of 10^{-24} seconds.The Δ states have mean masses of 1.232 GeV/c^2 and line widths, Γ, of 120 MeV/c^2. There may exist higher-mass baryon resonance states as well.

There are multiple charge states of nucleons, pions, and Δ particles. All Δ states have the same total isospin number and very similar masses. The different states are differentiated by charge and projected isospin number. This is true for nucleons and pions as well. Each Δ particle decays into a unique Nπ particle pair containing exactly one nucleon and one pion. The decay of a Δ particle into a Nπ pair must conserve charge, total isospin number, and projected isospin number.

In this paper, particles are represented by a Greek letter with the charge sometimes listed as a '++','+','0', or '-' symbol in the upper right index position as common convention requires ($\mathrm{Particle}^{\mathrm{Charge}}$). However, the convention omits any charge symbol for a proton (p) which has a '+1' charge. Sometimes a particle will be described in terms of a quantum mechanical isospin state in Dirac notation as follows:

$$\mathrm{Particle} \equiv |\mathrm{I}\,\mathrm{I_z}> \tag{3}$$

I represents the total isospin number and $\mathrm{I_z}$ represents the projected isospin number.

1.2 Reaction Channels

In the Table below, the resonance states are listed in order of descending isospin number and charge. The Δ^+ and Δ^0 resonance particles decay with asymmetric probability into two possible final Nπ states. In a resonance reaction the neutrinos interact with only one nucleon. The neutrino (ν_μ) or anti-neutrino ($\bar{\nu_\mu}$) become a muon (μ^-) or anti-muon (μ^+) respectively. The resonance states each represent a different eigenstate of projected isospin for a particle with total isospin $\frac{3}{2}$. Each projected isospin state can be decomposed into a superposition of a total isospin 1 state entangled with a total isospin $\frac{1}{2}$ state.

Initial State	**Final State**	**Isospin Breakdown**	**Final Products**	**100%**
ν_μp	$\mu^-\Delta^{++}$	$\Delta^{++} \equiv \lvert\frac{3}{2}\frac{3}{2}>=$		
		$\lvert\frac{1}{2}\frac{1}{2}> \lvert 11> \equiv \mathrm{p}\pi^+$	$\mu^-\mathrm{p}\pi^+$	1
ν_μn	$\mu^-\Delta^+$	$\Delta^+ \equiv \lvert\frac{3}{2}\frac{1}{2}>=$		
		$\sqrt{\frac{1}{3}}(\lvert\frac{1}{2}-\frac{1}{2}> \lvert 11> \equiv \mathrm{n}\pi^+)$	$\mu^-\mathrm{n}\pi^+$	$\frac{1}{3}$
		$+\sqrt{\frac{2}{3}}(\lvert\frac{1}{2}\frac{1}{2}> \lvert 10> \equiv \mathrm{p}\pi^0)$	$\mu^-\mathrm{p}\pi^0$	$\frac{2}{3}$
$\bar{\nu_\mu}$p	$\mu^+\Delta^0$	$\Delta^0 \equiv \lvert\frac{3}{2}-\frac{1}{2}>=$		
		$\sqrt{\frac{1}{3}}(\lvert\frac{1}{2}\frac{1}{2}> \lvert 1-1> \equiv \mathrm{p}\pi^-)$	$\mu^+\mathrm{p}\pi^-$	$\frac{1}{3}$
		$+\sqrt{\frac{2}{3}}(\lvert\frac{1}{2}-\frac{1}{2}> \lvert 10> \equiv \mathrm{n}\pi^0)$	$\mu^+\mathrm{n}\pi^0$	$\frac{2}{3}$
$\bar{\nu_\mu}$n	$\mu^+\Delta^-$	$\Delta^- \equiv \lvert\frac{3}{2}-\frac{3}{2}>=$		
		$\lvert\frac{1}{2}-\frac{1}{2}> \lvert 1-1> \equiv \mathrm{n}\pi^-$	$\mu^+\mathrm{n}\pi^-$	1

1.3 Experiments

Baryon resonances such as the Δ are detected indirectly. This is done by plotting the frequency of detecting a Nπ particle pair as a function of the detected invariant mass of the pair. A resonance state appears as a Breit-Wigner shaped enhancement in the distribution, centered on the invariant mass of the resonant state. For example, Δ states have masses of 1.232 GeV/c^2. When such a state decays into a Nπ pair, the two-body final state will have the same invariant mass. If the production of Nπ pairs is dominated by Δ decay, one expects to see a positive increase in the frequency of Nπ pairs around 1.232 GeV/c^2. An enhancement in Nπ invariant mass at a value higher than than 1.2 GeV/c^2 would suggest that there may exist resonance particles additional to the Δ particles. Many older experiments used bubble chambers to detect nueutrino-nucleon interactions. In a bubble chamber a moving charged particle ionizes the surrounding liquid and leaves a visable trajectory which can be imaged. The chamber is pervaded by a uniform magnetic feild. The length and curvature of a trajectory can be used to determine the mass, charge, and lifetime of the particle [6-12]. In *Review of Single Pion Production in Charged-Current Experiments for Evidence of Resonance Structure* I examined several papers on resonance production observed in bubble chamber experiments. I concluded that there was evidence for the creation of higher-mass baryon resonance particles. However, the possible contribution of higher resonance states to the resonance cross section has not yet been experimentally determined [5]. In this paper I turn to phenomenological models of baryon-resonance production to make further progress on this question.

1.4 The Axial Vector Mass and Form Factors

The other important question that this paper seeks to answer, in addition to the possible existence of higher mass resonance states, is the value of the axial vector mass (M_A) in the resonance reaction. In quantum feild theory (QFT) particles are understood to be quantized excitations of fields. A field assigns values to every space-time point. A scalar field assigns to every space-time point a single value (a scalar) and a vector field assigns every space-time point an array of values (a vector). A scalar particle is an excitation of a scalar field and a vector particle is an excitation of a vector field. There is another type of field known as an axial vector field. It follows that axial vector fields assign axial vectors to every space-time point and have quantized excitations known as axial vector particles. Axial vectors, like vectors, are one-dimensional arrays of numbers. However, axial vectors are distinguished from vectors by how they transform under parity inversion. An axial vector picks up an extra phase of '-1' under the operation of reflection [12].

A reaction can be interpreted as a transfer of energy and momentum from one field to another within a local area of space time. At the interaction site there are an uncountable number of virtual particles (briefly lived field excitations). The vector mass M_V is related to the masses of all the vector particles which exist at the interaction vertex. The axial vector mass M_A is the equivalent for the axial vector particles. The physical interpretation of M_A and M_V is however highly non trivial. M_V and M_A are parameters in the vector and axial vector form factors. The form factors are the fourier transforms of the scattering material

spacial distribution. They can be interpreted as the momentum space distribution of the scattering material. The generic dipole form factor is shown in equation 4.

$$F_{V,A} = \frac{F_0}{(Q^2 + M_{V,A}^2)^2} \tag{4}$$

The form factors characterize the structure of the interaction vertex. The form factors can be directly computed from a number of field propagators which in the context of QFT represent the probability amplitude for a transition from an initial state to a final state. A simple example of a propagator would be the probability amplitude of a virtual particle being created at one interaction site and propagating to another interaction site where it is annihilated. In this paper we can summarize the entire resonance reaction as a single transition amplitude for the incident nucleon to become a Δ particle. This transition amplitude can be expanded in terms of form factors. The dependence of the form factors to M_A and M_V relates them non-trivially to the virtual vector and axial vector particles respectively at the interaction vertex [12].

The value of M_V has been well-determined by experiments in electro-production which entirely involve vector fields. The vector field dynamics involved in neutrino-induced resonance production are thought to be highly similar to that of electro-production. Resonance reactions however also involve axial-vector field dynamics, the theory of which is far less established. The value of M_A has not been theoretically or experimentally determined. Recent estimates based on resonance production phenomenology place the value of M_A around 1.05 GeV/c^2. One of the major goals of this paper is to present new bounds on the possible values of M_A. This is done by treating M_A as an unknown parameter of the phenomenological models and then matching the model prediction as closely as possible to data.

1.5 Overview

In this paper I take phenomenological models of resonance production as the basis for a simulation of resonance production written in the computer language python. I review the phenomenological models and identify important form factors which contribute to the resonance cross section. I present the results of the code compared to GENIE, a widely used Monte Carlo event generator of neutrino-nucleon scattering. I also present the code itself in the hope that it will find future use and make the phenomenological models more accessible to future researchers. Finally, I discus the relevance of the results towards answering the two major questions explored in this paper, the existence of higher mass resonance states and the value of M_A.

2 Phenomenology

2.1 Historical Background

The Adler, model published in 1969, first explored the foundations of Δ-resonance production theory. The original paper covered all known single pion production channels: photon-

nucleon, electron-nucleon, and neutrino-nucleon scattering. The theory was derived from first principles of quantum field theory and the Feynman rules for calculating scattering amplitudes [1]. The theoretical model of Rein and Segal later expanded the original work of Adler. They modeled hadrons as quark harmonic oscillators to develop the form factors. The form factors appear in most models as coefficients that accompany kinematic terms in an expansion of the transition amplitude for a nucleon to turn into a Δ particle after having its total isospin number raised via an interaction with a neutrino. The transition amplitude can then be used to calculate the cross section of the neutrino-nucleon scattering. The cross section can often be expanded in terms of polarization/helicity states of the Δ particle [2]. The model of Rein and Segal serves as the basis for baryon-resonance production events within the GENIE Monte Carlo simulation. In 2005, Emmanuel A. Pascos published a detailed phenomenological model of resonance production which combined elements from the earlier theoretical models with considerations derived from experimental data. The objective of the Pascos model was to explain the results of several neutrino experiments such as those at ANL, BNL, K2K, and MiniBooNE [3,4].

The vector form factors were taken from the earlier theoretical models. The axial vector form factors are less well established within the theory so Pascos put phenomenological form factors in by hand to best match the data. The vector form factors can be derived using the well-established conserved vector current hypothesis which places strict constraints on vector field dynamics. The theory for axial vector form factors is less rigorous. The widely accepted but approximate partially conserved axial vector current hypothesis PCAC places some constraints on the form factors. The PCAC hypothesis along with experimental data allowed Pascos to develop his phenomenological model of baryon resonance production [3,4]. This paper uses the model of Pascos to develop a simulation of resonance production. The Pascos model is more modern then the Rein-Segal model so it is potentially more robust. However, the modified Rein-Segal model built into GENIE is still predominately used by the neutrino physics community. It is the hope of this paper, in addition to answering questions about higher mass resonance states and the value of M_A, to also make the Pascos model more accessible to the neutrino physics community by presenting a usable simulation based on that model.

2.2 Reaction Kinematics

The Pascos paper introduces the phenomenology of one particular reaction channel. Adjacent to each symbol representing a particle is a four-vector in parenthesis which represents the four-momentum of the particle. The length of a four-vector, calculated using the Minkowski metric signature (1,-1,-1,-1), is the invariant mass of a particle. The symbol 'q' represents the four-momentum transfer from the lepton current to the hadronic current. The neutrinos and muons are part of the lepton current while the nuclear particles are part of the hadronic current. All calculations are done in the rest frame of the incident nucleon and in natural units. The initial 3-momentum of the proton is zero and the energy of the proton is just the rest mass of the proton. The neutrino has a negligible mass. It is possible to calculate the inner products of several important four-vectors in terms of proton mass (m_N), the four-

momentum transfer (Q^2), the neutrino energy (E), and the invariant mass of the resonance particle (W).

$$\nu(\vec{k})p(\vec{p}) \rightarrow \mu^-(\vec{k'})\Delta^{++}(\vec{p'}) \rightarrow \mu^- p\pi^+$$

$$q = k - k', \qquad Q^2 = -q^2, \qquad W^2 = p'^2$$

$$k \cdot p = m_N E, \quad q \cdot p = m_N \nu, \quad \nu = \frac{W^2 + Q^2 - m_N^2}{2m_N}$$

$$p \cdot p' = \frac{1}{2}(W^2 + Q^2 + m_N^2), \quad q \cdot p' = m_N \nu - Q^2.$$

The double differential cross section can be calculated using the lepton tensor ($L_{\mu\nu}$) and the hadronic tensor ($W^{\mu\nu}$). The lepton tensor is calculated using the lepton four-momentum vectors. The gamma matrices are the standard Dirac matrices. The 'W_i' are known as the structure functions. The hadronic tensor can be calculated from the hadronic four-momentum vectors and from the structure functions.

$$\frac{d\sigma}{dQ^2 dW} = \frac{\pi W}{m_N E E'} \frac{G^2}{16\pi^2} \cos^2\theta_C \frac{E'}{E} L_{\mu\nu} \mathcal{W}^{\mu\nu}$$

$$\begin{aligned} L_{\mu\nu} &= \mathrm{Tr}[\gamma_\mu(1-\gamma_5)\not{k}\gamma_\nu \not{k}'] \\ &= 4(k_\mu k'_\nu + k_\nu k'_\mu - g_{\mu\nu} k \cdot k' - i\varepsilon_{\mu\nu\alpha\beta} k^\alpha k'^\beta) \end{aligned}$$

$$\begin{aligned} \mathcal{W}^{\mu\nu} = &-\mathcal{W}_1 g^{\mu\nu} + \frac{\mathcal{W}_2}{m_N^2} p^\mu p^\nu - i\varepsilon^{\mu\nu\sigma\lambda} p_\sigma q_\lambda \frac{\mathcal{W}_3}{2m_N^2} \\ &+ \frac{\mathcal{W}_4}{m_N^2} q^\mu q^\nu + \frac{\mathcal{W}_5}{m_N^2}(p^\mu q^\nu + q^\mu p^\nu) \\ &+ i\frac{\mathcal{W}_6}{m_N^2}(p^\mu q^\nu - q^\mu p^\nu) \end{aligned}$$

The hadronic tensor can be alternatively calculated as shown below. The calculation sums the transition probability of a proton becoming a Δ particle for all polarization states of the Δ particle ($\bar{\psi}_\gamma$). The calculation is done assuming a random value of invariant mass of the Δ particle (W). Note here that the value of W is not fixed but rather can vary over a small range. Final calculations have to integrate over all values of W. M_R refers to the central mass value within the range of possible values for W. The $\delta(W^2 - M_R^2)$ function, known as the resonance width, is distributed around M_R which can be interpreted as the probability that the Δ particle will have an invariant mass W.

$$\mathcal{W}^{\mu\nu} = \frac{1}{2m_N}\sum\langle p|J^{\mu}(0)|\Delta\rangle\langle\Delta|J^{\nu}(0)|p\rangle\delta(W^2 - M_R^2)$$

$$\delta(W^2 - M_R^2) = \frac{M_R\Gamma_R}{\pi}\frac{1}{(W^2 - M_R^2)^2 + M_R^2\Gamma_R^2}$$

$$\langle\Delta^{++}|J^{\nu}|p\rangle = \sqrt{3}\bar{\psi}_{\lambda}(p')d^{\lambda\nu}u(p)$$

The hadronic tensor can be alternatively calculated using the $S^{\sigma\lambda}$ projection operator which projects onto a basis of Δ polarization states. The latter two methods of calculating the hadronic tensor rely on $d^{\lambda\nu}$ tensor.

$$\mathcal{W}^{\mu\nu} = \frac{3}{2}\frac{1}{2m_N}Tr[(\bar{d})^{\mu\sigma}S_{\sigma\lambda}d^{\lambda\nu}(\not{p} + m_N)]\delta(W^2 - M_R^2)$$

$$|\psi_{\Delta}\rangle\langle\psi_{\Delta}| = S^{\sigma\lambda} = [\not{p}' + M_R]\left[-g^{\sigma\lambda} + \frac{1}{3}\gamma^{\sigma}\gamma^{\lambda} + \frac{1}{3M_R}\times(\gamma^{\sigma}p'^{\lambda} - p'^{\sigma}\gamma^{\lambda}) + \frac{2}{3M_R^2}p'^{\sigma}p'^{\lambda}\right]$$

The $d^{\lambda\nu}$ tensor is composed of terms known as form factors (C_i). At the interaction vertex there are a series of processes that can be categorized as either involving vector or axial-vector fields. The C^V form factors relate to processes in the vector fields and the C^A form factors relate to processes in the axial-vector fields.

$$d^{\lambda\nu} = g^{\lambda\nu}\left[\frac{C_3^V}{m_N}\not{q} + \frac{C_4^V}{m_N^2}(p'\cdot q) + \frac{C_5^V}{m_N^2}(p\cdot q) + C_6^V\right]\gamma_5 - q^{\lambda}\left[\frac{C_3^V}{m_N}\gamma^{\nu} + \frac{C_4^V}{m_N^2}p'^{\nu} + \frac{C_5^V}{m_N^2}p^{\nu}\right]\gamma_5$$
$$+ g^{\lambda\nu}\left[\frac{C_3^A}{m_N}\not{q} + \frac{C_4^A}{m_N^2}(p'\cdot q)\right] - q^{\lambda}\left[\frac{C_3^A}{m_N}\gamma^{\nu} + \frac{C_4^A}{m_N^2}p'^{\nu}\right] + g^{\lambda\nu}C_5^A + q^{\lambda}q^{\nu}\frac{C_6^A}{m_N^2}.$$

The vector form factors are determined using both experimental data and first principles. Each form factor is associated to a specific kinematic procses at the interaction vertex. The conserved vector-current hypothesis eliminates all vector form factors exept for the third and fourth terms. The fourth term can be determined as a function of the third term. The third vector form factor is determined using electro-production experiments that have been studied in depth. The dominance of specific electric multi-pole moments have been determined for electro-production experiments. Vector form factors dominate electro-production experiments which is why the results of those experiments can be used to set the vector form factors in this model. The axial vector form factors are less established experimentally and theoretically. The PCAC hypothesis helps eliminate some of the axial vector form factors. The Pascos paper proposes a form for the 5^{th} axial vector form factor based on matching the model to the data. The other form factors can be determined from the 5^{th} axial vector form factor.

$$C_3^V(Q^2) = \frac{C_3^V(0)}{(1+Q^2/M_V^2)^2}\frac{1}{1+Q^2/4M_V^2}\ ,\ C_4^V = -C_3^V\frac{m_N}{W}$$
$$C_5^A(Q^2) = \frac{C_5^A(0)}{(1+Q^2/M_A^2)^2}\frac{1}{1+Q^2/3M_A^2}\ ,\ C_4^A = -\frac{C_5^A}{4}\ ,\ C_6^A = C_5^A\frac{m_N^2}{Q^2+m_\pi^2}$$

The equations below present a separate method of calculating the double differential cross section. This equality bypasses the need to explicitly calculate the leptonic tensor and the hadronic tensor. This equation allows the double differential cross section to be calculated directly from the structure functions. The structure functions are calculated from the form factors which are calculated from the four vectors. This was selected as the method for calculating the double differential cross section in the simulation [4].

$$\begin{aligned}\frac{d\sigma}{dQ^2dW} = \frac{G^2}{4\pi}\cos^2\theta_C\frac{W}{m_N E^2}\Bigg\{&\mathcal{W}_1(Q^2+m_\mu^2)\\ &+\frac{\mathcal{W}_2}{m_N^2}\left[2(k\cdot p)(k'\cdot p)-\frac{1}{2}m_N^2(Q^2+m_\mu^2)\right]\\ &-\frac{\mathcal{W}_3}{m_N^2}\left[Q^2k\cdot p-\frac{1}{2}q\cdot p(Q^2+m_\mu^2)\right]\\ &+\frac{\mathcal{W}_4}{m_N^2}m_\mu^2\frac{(Q^2+m_\mu^2)}{2}-2\frac{\mathcal{W}_5}{m_N^2}m_\mu^2(k\cdot p)\Bigg\}\end{aligned}$$

3 Building the Model

3.1 Logical Structure of the Model

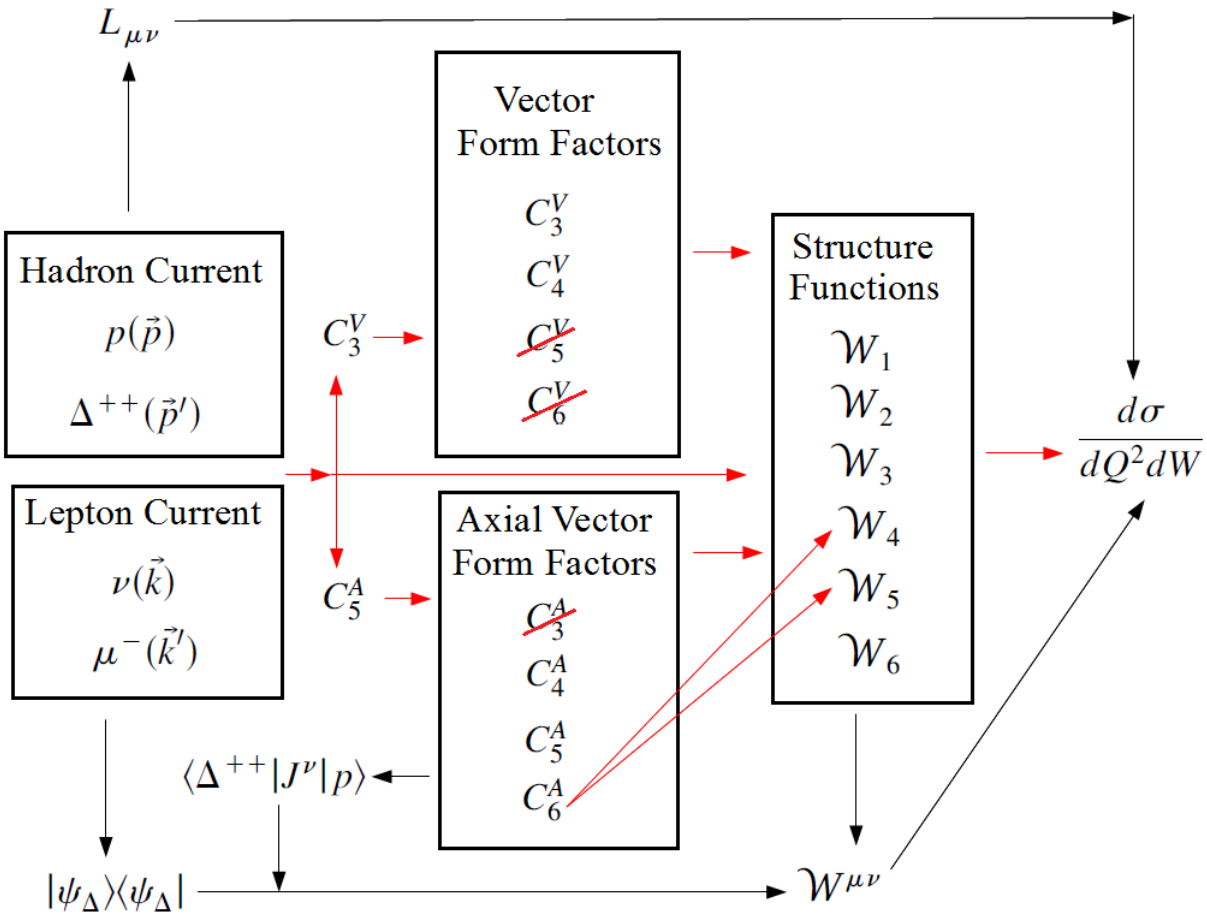

Figure 1: Schematic summary of the Pascos model. An arrow connecting one object in the model to another indicates that the former appears in an expansion of the latter. There are multiple possible algorithms for calculating the double differential cross section. The red arrows represent the method I used to build my simulation.

Above I present a schematic summary of the Pascos model. The arrows show which objects within the model can be used to calculate other objects. All form factors appear in all structure functions except for C_6^A which appears only within W_4 and W_5. The conserved vector current hypothesis eliminates C_5^V and C_4^V. The partial conserved axial-vector current hypothesis eliminates C_3^A. The remaining vector form factors can be calculated using C_3^V and the remaining axial vector form factors can be calculated from C_5^A. The C_3^V and C_5^A form factors are the most important form factors. The structure functions depend upon vector and axial vector form factors. W_3 is unique in that it is entirely dependent on interference

terms. No other structure function has any dependence on interference terms. Interference terms are the products of terms including both vector and axial-vector form factors and represent interference between the vector and axial-vector fields. This is why the label of W_3 can be substituted with the label 'I" which stands for 'interference.'

The inputs to the model are the four vectors for the particles. The goal is always to calculate the double differential cross section with respect to Q^2 and W, $\frac{d\sigma}{dWdQ^2}$. The double differential cross section is a function of E as well as W and Q^2. There are multiple methods of calculating this final result. The red arrows show the method that I used to build the simulation. The four vectors are used to calculate the form factors which are in turn used to calculate the structure functions. The structure functions are then used to calculate the double differential cross section. The lepton tensor, hadron tensor, polarization projection operator, and transition amplitude are never explicitly calculated.

3.2 Integration Limits

For particular values of E, Q^2, and W, we can calculate the four vectors, form factors, structure functions, and finally the double differential cross section $\frac{d\sigma}{dWdQ^2}$. To get the single differential crossection over Q^2 alone, we integrate over W. The lower bound for W integration is fixed at the mass of the nucleon m_N plus the mass of the pion m_π. The upper bound is depends on the value of Q^2. This means that for a given value of Q^2, the range of W values over which we must calculate $\frac{d\sigma}{dWdQ^2}$ depends on that value of Q^2.

$$W_-(Q^2) = m_N + m_\pi,$$

$$W_+^2(Q^2) = \left[\frac{1}{4}s^2a_-^2\left(\frac{m_\mu^4}{s^2} - 2\frac{m_\mu^2}{s}\right) - \left(Q^2 + \frac{1}{2}m_\mu^2 a_+^2\right)^2 + sa_-\left(Q^2 + \frac{m_\mu^2}{2}a_+\right)\right]/[a_-(Q^2 + m_\mu^2)],$$

$$s = 2m_N E + m_N^2,\ a_\pm = 1 \pm m_N^2/s$$

To then find the value of the cross section at a specific energy, we perform a second integration over Q^2. The final cross section is achieved by integrating the double differential cross section over both Q^2 and W. The bounds on Q^2 are put in by hand. In this paper I set the lower limit of Q^2=0 GeV^2 and the upper limit at 2.0 GeV^2. This was based on considerations of the range over which the Pascos model is viable.

$$\frac{d\sigma}{dQ^2}(E, Q^2) = \int_{W_-}^{W_+} \frac{d\sigma}{dWdQ^2}(E, W, Q^2)dW \tag{5}$$

$$\sigma(E) = \int_{0.0}^{2.0} \frac{d\sigma}{dQ^2}(E, Q^2)dQ^2 \tag{6}$$

3.3 Flux Weighting

The differential cross section as calculated in Eq.(4), gives the expected number or resonance events at a given value of Q^2 if the neutrino beam has a fixed energy of E. However, the

neutrino beam produces a flux over a range of energy values. The flux function used in this paper is that of the MINERvA neutrino beam.

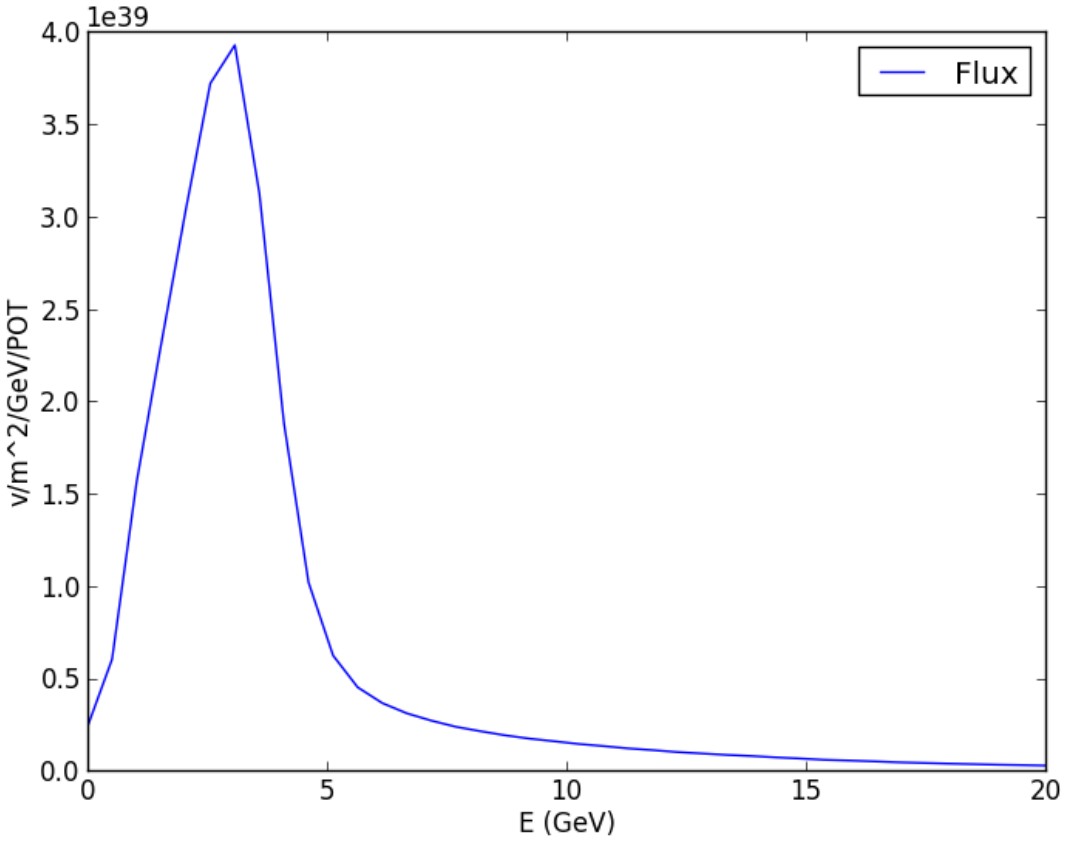

Figure 2: Neutrino beam flux as a function of neutrino energy (E). The beam peaks around 3.0 GeV.

I am interested in calculating the effective differential cros section $\frac{d\sigma^{'}}{dQ^2}(Q^2)$ which is only a function of Q^2. It relates to the actual number of expected resonance reactions at a given value of Q^2. $\frac{d\sigma^{'}}{dQ^2}(Q^2)$ is calculated by taking a flux weighted integration of $\frac{d\sigma}{dQ^2}(E, Q^2)$ over E. In this paper I study data in a neutrino energy range of 1.5 to 4.0 GeV.

$$\frac{d\sigma^{'}}{dQ^2}(Q^2) = \int_{1.5}^{4.0} \text{flux(E)} * \frac{d\sigma}{dQ^2}(E, Q^2)dE \tag{7}$$

3.4 Pauli Blocking

The Pauli suppression factor is a possible correction to baryon resonance production models. So far we have examined the phenomenology of resonance production involving only a single

nucleon. We are interesting in determine the phenomenology of resonance production when the incident nucleon is within the nuclear medium of an atomic nucleus. Experiments suggest that the Δ particle decays inside the atomic nucleus. This makes sense with respect to modern theory on the Δ particles. The lifetime of the Δ particle is too short for there to be a significant probability of the Δ particle escaping the nucleus within its lifetime at the energy scales we are exploring. The Δ particle decays into a pion and a nucleon within the nucleus. Nucleons are fermions, so the newly created nucleon from the decay of the Δ particle cannot enter a momentum state already occupied by another nucleon within the nucleus. Theoretically, Δ resonance production may be suppressed if there are no unoccupied momentum states for the nucleon produced by decay to enter. The nucleons in the atomic nucleus have relatively low momentum so the suppression of Δ resonance production should be highest at low Q^2 and diminish rapidly at high Q^2.

$$q_\pi(W) = (1/2W)[(W^2 - M^2 - m_\pi^2)^2 - 4M^2 m_\pi^2]^{1/2}$$

$$p_\pi = \frac{W^2 + m_\pi^2 - M^2}{2W}, \quad q_0 = \frac{W^2 - M^2 - Q^2}{2W} \quad \text{and} \quad R = p_F .$$

(i) For $2p_F \geq |\vec{q}| + p_\pi > |\vec{q}| - p_\pi$

$$g(W, |\vec{q}|) = \frac{1}{2|\vec{q}|}\left(\frac{3|\vec{q}|^2 + p_\pi^2}{2R} - \frac{5|\vec{q}|^4 + p_\pi^4 + 10|\vec{q}|^2 q_\pi}{40R^3}\right)$$

(ii) For $|\vec{q}| + p_\pi > 2p_F$

$$g(W, |\vec{q}|) = \frac{1}{4p_\pi|\vec{q}|}\left((|\vec{q}| - p_\pi)^2 - \frac{4}{5}R^2 - \frac{(|\vec{q}| - p_\pi)^3}{2R} + \frac{(|\vec{q}| - p_\pi)^5}{40R^3}\right)$$

(iii) For $|\vec{q}| - p_\pi \geq 2p_F \qquad g(W, |\vec{q}|) = 1$

Here, g(W, |q|) is the Pauli suppression factor. P_F is the Fermi momentum which is related to the average momentum of the background nucleons within the nucleus [3].

4 Results

I calculated the contribution of various parts of the model to the double differential cross section $\frac{d\sigma}{dQ^2}$. I present the results for $E_\nu = 4.0$ GeV, which is slightly above the peak of the neutrino flux. For $M_A = 1.1$ GeV and $M_A = 1.3$ GeV, I got good agreement between the Pascos model and the prediction of the GENIE Monte Carlo event generator.

4.1 Form Factors

The contribution of the form factors to $\frac{d\sigma}{dQ^2}$ was calculated. The first plot shows the primary form factors of interest. The curve labelled V3 represents the contribution to the cross section of C_3^V, A5 represents the contribution of C_5^A, and V3-A5 represents the contribution of the interference between C_3^V and C_5^A. The total double differential cross section is the direct sum of the contributions from all the form-factor terms. V3 is the sum of all terms in $\frac{d\sigma}{dQ^2}$ which contain C_3^V but no other form factors. The same is true for A5 and C_5^A respectively. V3-A5 is the sum of all terms in $\frac{d\sigma}{dQ^2}$ which contain the product $C_3^V C_5^A$ but no other form factors or form factor products. C_3^V represents the most significant processes in the vector fields and all other vector form factors depend on it, same for C_5^A with respect to the axial vector fields and form factors, and the product $C_3^V C_5^A$ represents the interaction between these vector and axial vector processes.

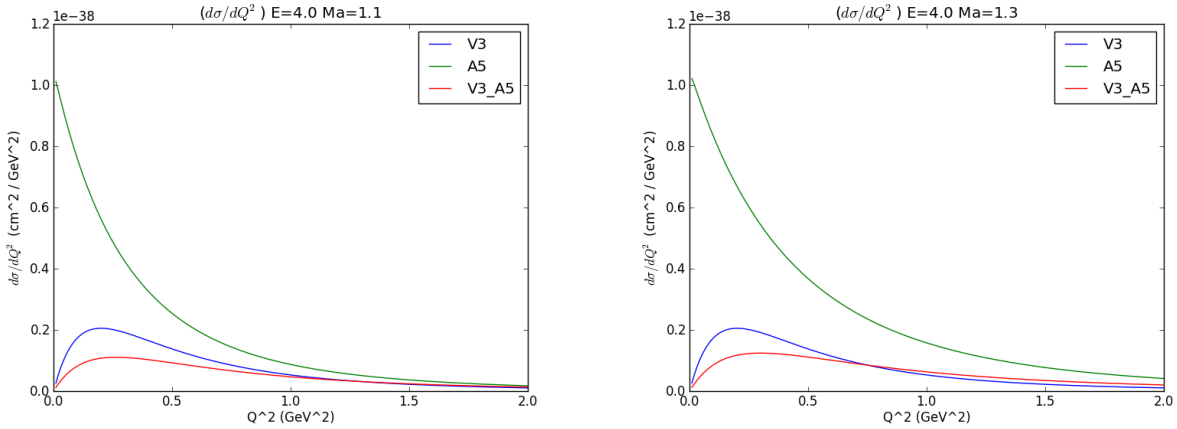

Figure 3: Primary form factor contributions of interest calculated for M_A values of 1.1 and 1.3 GeV/c^2.

The term A5 has the biggest contribution to $\frac{d\sigma}{dWdQ^2}$ which suggests that the resonance reaction is dominated by axial vector field dynamics. V3 and V3 – A5 have comparable contributions with V3 slightly larger in the low Q^2 region but dying off faster at higher Q^2. All contributions have low Q^2 fall-off which means that they go to 0 at Q^2=0. This behavior was observed for all contributions though it may be difficult to see for A5.

The next plots show the rest of the form factor contributions $\frac{d\sigma}{dQ^2}$. Most of the contributions are negative. All of the contributions are of lower magnitude than V3, A5, and V3-A5. This explains why C_3^V, C_5^A, and their interaction are of primary interest. They give the most significant contribution.

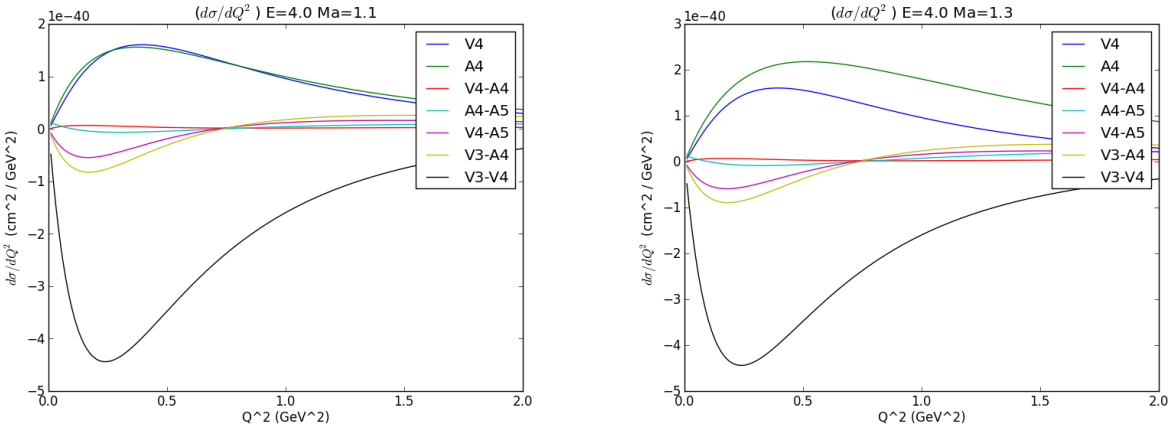

Figure 4: Form factor contributions calculated for M_A values of 1.1 and 1.3 GeV/c^2.

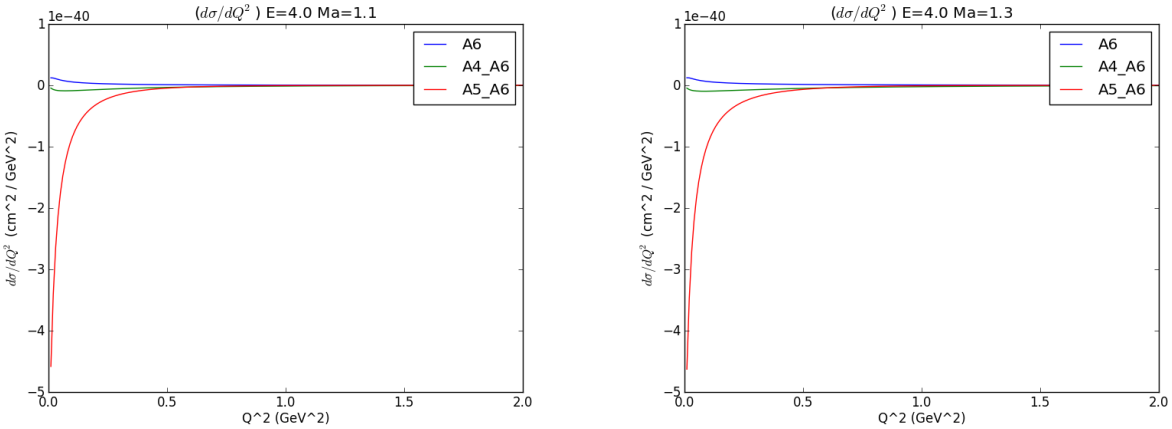

Figure 5: Form factor contributions calculated for M_A values of 1.1 and 1.3 GeV/c^2.

4.2 Structure Functions

The contribution of the structure functions to $\frac{d\sigma}{dQ^2}$ was calculated. The functions labeled 'Wn' refer to the n structure function contributions. 'CS' refers to the differential cross section $\frac{d\sigma}{dQ^2}$. The following plot allows for a comparison between the structure function contributions and the total cross section. The structure function W2 is heavily dominated by axial vector form factor terms, W1 is dominated by vector form factor terms, and W3 contains all interaction form factor terms. W5 and W4 are the only structure functions which includes contributions from C_6^A.

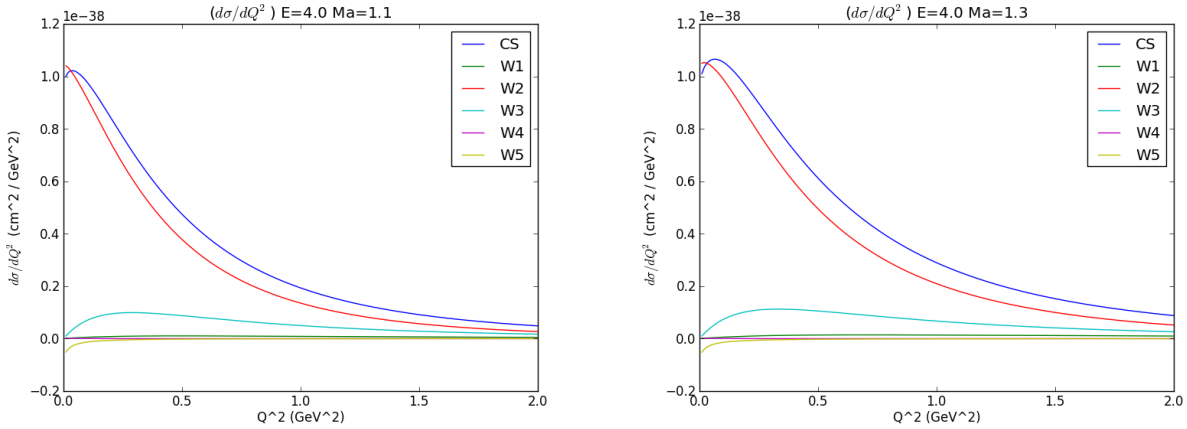

Figure 6: Structure function contributions for M_A values of 1.1 and 1.3 GeV/c^2.

4.3 Double Differential Cross Section

The double differential cross section $\frac{d\sigma}{dWdQ^2}$ was calculated. The value of the double differential cross section is presented in natural units.

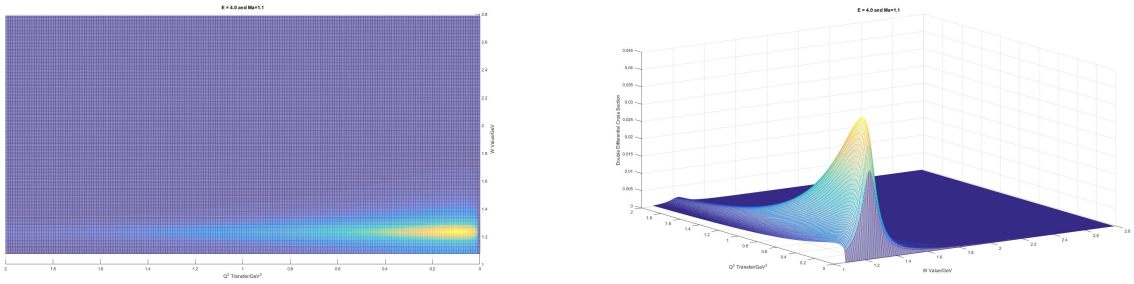

Figure 7: Double differential cross section plots for E = 4.0 GeV and M_A = 1.1 GeV/c^2 over W and Q^2, shown from above and from an angle.

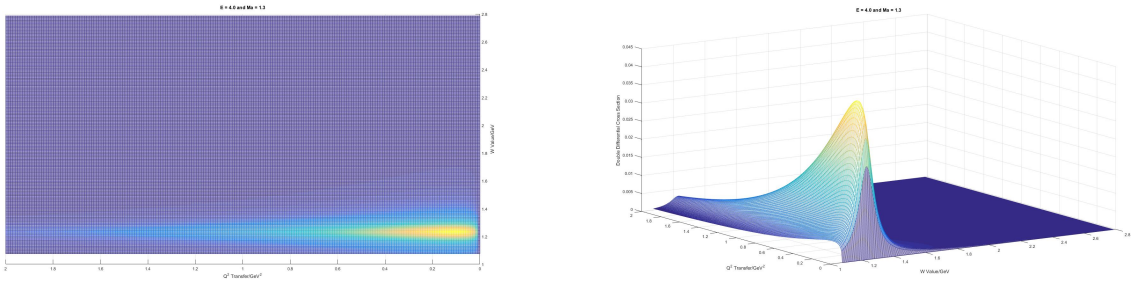

Figure 8: Double differential cross section plots for E = 4.0 GeV and M_A = 1.3 GeV/c^2 over W and Q^2, shown from above and from an angle.

4.4 Differential Cross Section

The following plots show the differential cross section $\frac{d\sigma}{dQ^2}$, the total axial vector contribution (A), the total vector contribution (v), and the total interference contribution (I). V represents the sum of all vector form factor contribution terms, A represents the sum of all axial vector form factor contribution terms, and I represents the sum of all interference form factor contributions which is just the third structure function W3. The term V is dominated by V3, A is dominated by A5, and I is dominated by V3-A5. The total cross section is highly axial-vector dominated.

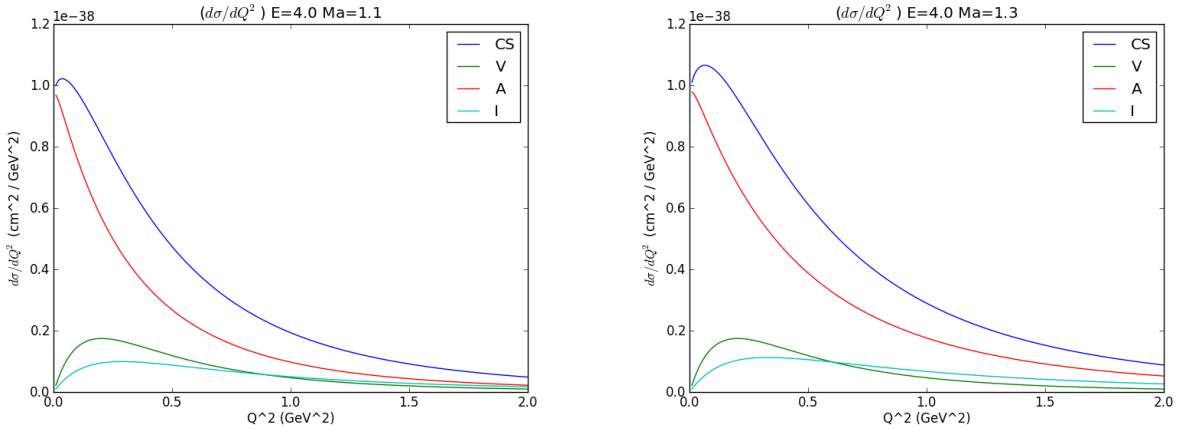

Figure 9: Differential cross section for M_A values of 1.1 and 1.3 GeV/c^2.

The next plots show a comparison to the differential cross section (CS) to the differential cross section with Pauli suppression turned on (CS-PE). We see a reduction in $\frac{d\sigma}{dQ^2}$ at low Q^2 values. This is the expected effect of Pauli suppression.

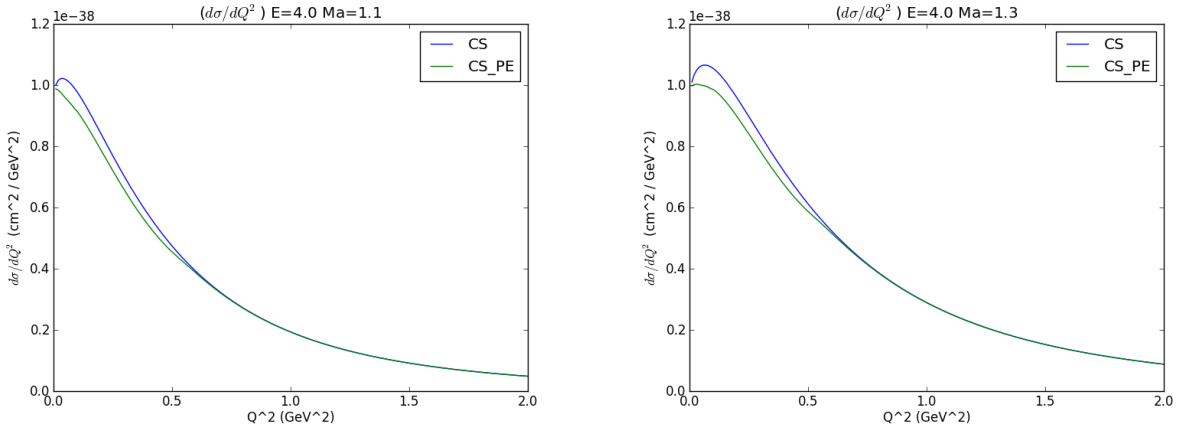

Figure 10: Comparison of differential cross section with and without Pauli supression for M_A values of 1.1 and 1.3 GeV/c^2 respectively.

4.5 Cross Section

Integrating $\frac{d\sigma}{dQ^2}$ gives σ(E) which is shown in the plot below. The cross section levels off around 1.75 GeV. The terms V, A, and I again represent the vector, axial vector, and interference contributions to the cross section respectively. A is larger showing that the cross section is axial vector dominated. A and V continue to grow as energy increases. Interestingly I dies off at higher energy values which leads to the leveling off of σ(E) and suggests a de-coupling of vector and axial vector processes at higher energy values. CS-PE is the cross section when Pauli suppression is turned on. The effect of Pauli suppression is a small reduction in the cross section at all energy values.

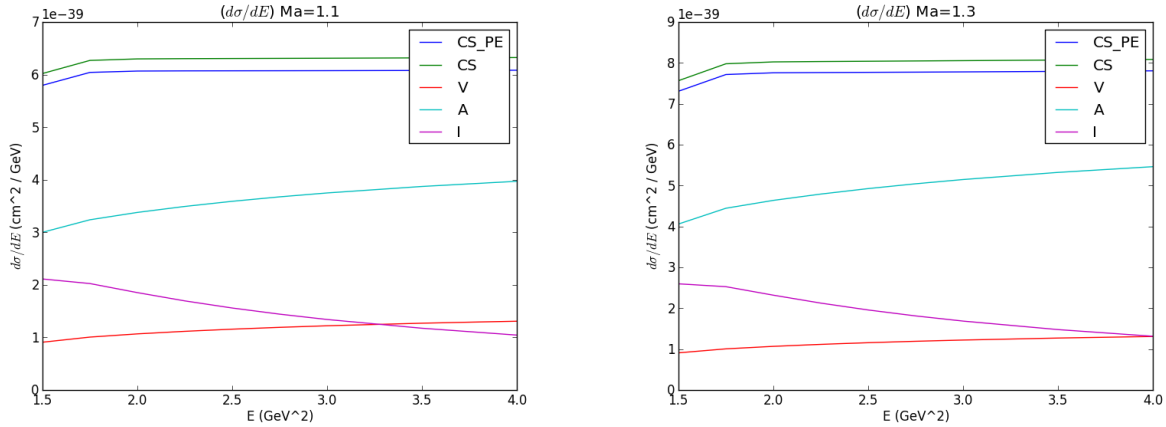

Figure 11: Cross section as a function of energy for M_A values of 1.1 and 1.3 GeV/c^2 respectively.

4.6 Effective Differential Cross Section

The next plot shows the flux-weighted energy-integrated differential cross section $\frac{d\sigma}{dQ^2}(Q^2)$. As M_A increases, the peak shifts to a slightly higher Q^2 value and the high Q^2 decay becomes slower.

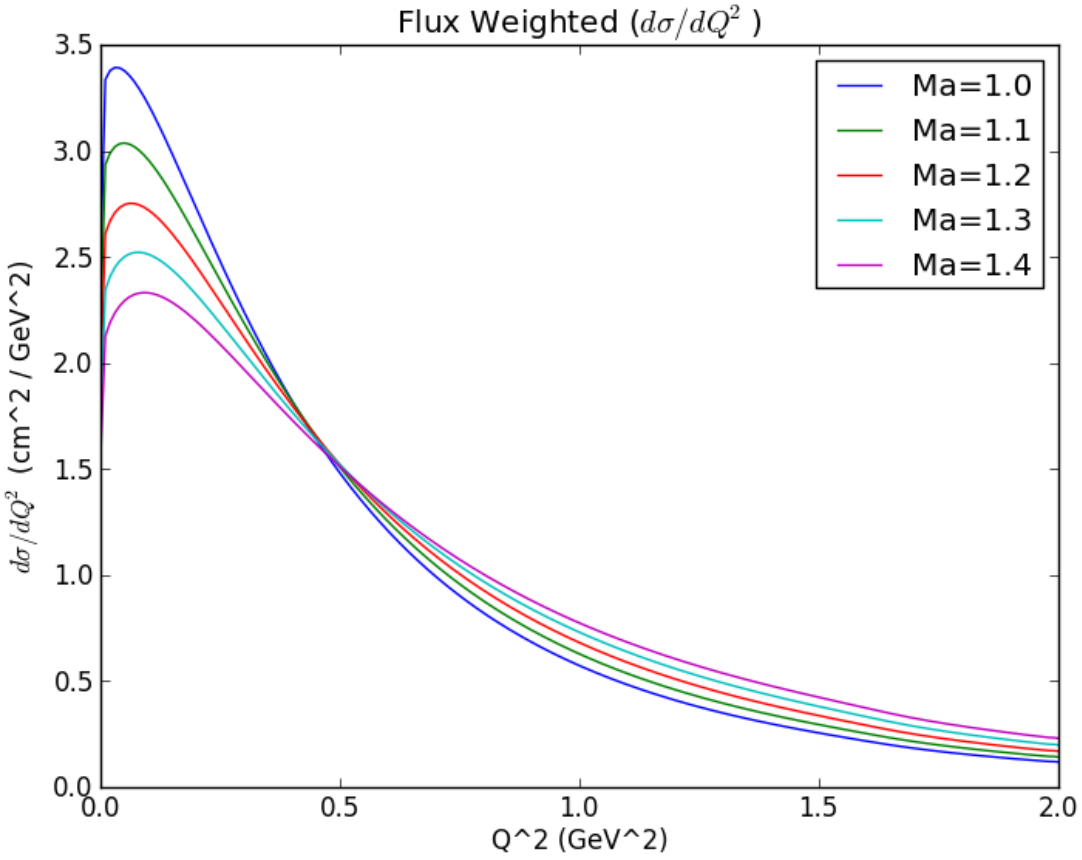

Figure 12: Flux-weighted differential cross section at M_A values of 1.1, 1.2, 1.3 and 1.4 GeV/c^2. The y-axis scale is arbitrary and all curves are area normalized. As M_A increases the high Q^2 becomes slower.

I am now interested in matching $\frac{d\sigma}{dQ^2}(Q^2)$ against the prediction of the GENIE event generator. I received GENIE generated plots for reaction event rate as a function of Q^2 for both mixed resonance (RES) and pure Δ (Delta) samples. These plots came courtesy of private communications I had with a MINERvA experimentalist collaborator who had already calibrated GENIE to match the most recent experimental data.

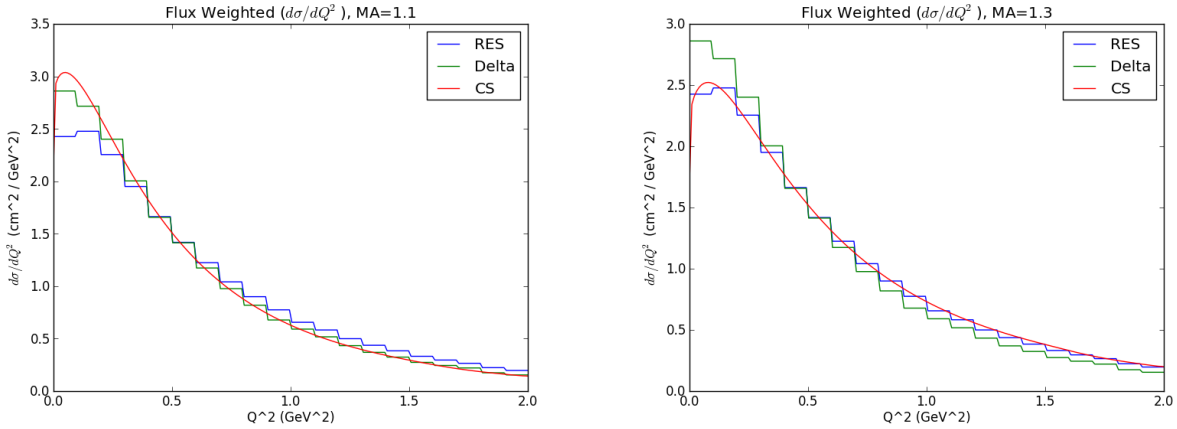

Figure 13: Flux-weighted differential cross section compared to GENIE plots at M_A values of 1.1 and 1.3 GeV/c^2 respectively. RES is the GENIE prediction for mixed baryon resonance production and Delta is the GENIE prediction for Δ baryon resonance production only. The simulation curves are area normalized.

The model matched with the Delta plot most closely at $M_A = 1.1$ GeV/c^2 and matched with the RES plot most closely at 1.3 GeV/c^2.

5 Discussion

In trying to match the model to GENIE I did not find it useful to turn on the Pauli exclusion factor. This factor is often left out of phenomenological models of resonance production and I have not found any evidence that it should be included. An M_A value of 1.1 GeV^2 is close to what M_A is expected to be in the literature [4]. Therefore, I have confirmed that the Pascos model is indeed consistent with GENIE for modelling baryon resonance production. The fact that the model matched the GENIE prediction for mixed resonance events is very interesting. Assuming the accuracy of GENIE for modeling higher mass resonance production, it shows that a crude approximation of mixed resonance production can be achieved by raising the value of M_A within a model designed for Δ resonance production only. It shows that we can find an effective value of axial vector mass, $M_{A\text{–effective}}$, and treat a resonance reaction involving multiple resonance states as though it only involved a single resonance state with $M_{A\text{–effective}}$. The higher mass resonance states in a mixed resonance reaction pull $M_{A\text{–effective}}$ above 1.1 GeV^2 which is the $M_{A\text{–Delta}}$ value.

6 Acknowledgments

I would like to thank Professor Anthony Mann, Professor Hugh Gallagher, and the rest of the Experimental High Energy Research group at Tufts University for advising me throughout my time working on this project. I would also like to thank Ozgur Altinok, a member of the Tufts experimental HEP group, for providing access to his GENIE event samples

which appear in this paper. These GENIE plots were calibrated to model real data from the MINERvA experiments at Fermilab. Also, I would like to thank Saqib Shadman for preparing the plots of the double differential cross section.

7 Appendix A: Structure Functions

This Appendix contains the equations which allow the structure functions to be calculated from the form factors. The V_i's are functions of the four vectors and Q^2. The structure functions are then obtained by multiplying the V_i functions by the δ function [4].

$$\frac{V_1}{3} = \frac{(C_3^V)^2}{m_N^2}\frac{2}{3M_R^2}[(q\cdot p - Q^2)^2(q\cdot p + m_N^2) + M_R^2((q\cdot p)^2 + Q^2 m_N^2 + Q^2 m_N M_R)] + \frac{(C_4^V)^2}{m_N^4}\frac{2}{3}(q\cdot p - Q^2)^2$$
$$\times (q\cdot p + m_N^2 - m_N M_R) + \frac{C_3^V C_4^V}{m_N^3}\frac{2}{3M_R}(q\cdot p - Q^2)[(q\cdot p - Q^2)(q\cdot p + m_N^2 - 2m_N M_R) + M_R^2 q\cdot p]$$
$$+\frac{2}{3}\left[\left(\frac{C_4^A}{m_N^2}\right)^2(q\cdot p - Q^2)^2 + (C_5^A)^2 + 2\frac{C_4^A C_5^A}{m_N^2}(q\cdot p - Q^2)\right][q\cdot p + m_N^2 + m_N M_R]$$

$$\frac{V_2}{3} = (C_3^V)^2\frac{2}{3M_R^2}Q^2[q\cdot p + m_N^2 + M_R^2] + \frac{(C_4^V)^2}{m_N^2}\frac{2}{3}Q^2[q\cdot p + m_N^2 - m_N M_R] + \frac{C_3^V C_4^V}{m_N}\frac{2}{3M_R}Q^2[q\cdot p + (M_R - m_N)^2]$$
$$+\frac{2}{3}\left[(C_5^A)^2\frac{m_N^2}{M_R^2} + \frac{(C_4^A)^2}{m_N^2}Q^2\right][q\cdot p + m_N^2 + m_N M_R]$$

$$\frac{V_3}{3} = \frac{4}{3M_R}\left[-\frac{C_3^V C_4^A}{m_N}(q\cdot p - Q^2) - C_3^V C_5^A m_N\right][2M_R^2 + 2m_N M_R + Q^2 - q\cdot p] + \frac{4}{3}(q\cdot p - Q^2)$$
$$\times\left[-\frac{C_4^V C_4^A}{m_N^2}(q\cdot p - Q^2) - C_4^V C_5^A\right]$$

$$\frac{V_4}{3} = \frac{2}{3M_R^2}(C_3^V)^2[(2q\cdot p - Q^2)(q\cdot p + m_N^2) - M_R^2(m_N^2 + m_N M_R)] + \frac{2}{3}\frac{(C_4^V)^2}{m_N^2}(2q\cdot p - Q^2)[q\cdot p + m_N^2 - m_N M_R]$$
$$+\frac{2}{3M_R}\frac{C_3^V C_4^V}{m_N}[(2q\cdot p - Q^2)(q\cdot p + m_N^2 - 2m_N M_R) + q\cdot p M_R^2] + \frac{2}{3}\left[(C_5^A)^2\frac{m_N^2}{M_R^2} + \frac{(C_4^A)^2}{m_N^2}(2q\cdot p - Q^2)\right.$$
$$\left.+\frac{(C_6^A)^2}{m_N^2 M_R^2}((Q^2 - q\cdot p)^2 + Q^2 M_R^2) + 2C_4^A C_5^A - 2\frac{C_4^A C_6^A}{m_N^2}q\cdot p - 2\frac{C_5^A C_6^A}{M_R^2}(M_R^2 + Q^2 - q\cdot p)\right]$$
$$\times[q\cdot p + m_N^2 + m_N M_R]$$

$$\frac{V_5}{3} = \frac{2}{3}\frac{(C_3^V)^2}{M_R^2}q\cdot p[q\cdot p + m_N^2 + M_R^2] + \frac{2}{3}\frac{(C_4^V)^2}{m_N^2}q\cdot p[q\cdot p + m_N^2 - m_N M_R] + \frac{2}{3M_R}\frac{C_3^V C_4^V}{m_N}q\cdot p[q\cdot p + (M_R - m_N)^2]$$
$$+\frac{2}{3}\left[\frac{(C_4^A)^2}{m_N^2}q\cdot p + (C_5^A)^2\frac{m_N^2}{M_R^2} + C_4^A C_5^A - \frac{C_4^A C_6^A}{m_N^2}Q^2 + \frac{C_5^A C_6^A}{M_R^2}(q\cdot p - Q^2)\right][q\cdot p + m_N^2 + m_N M_R]$$

$$\mathcal{W}_i(Q^2,\nu) = \frac{1}{m_N}V_i(Q^2,\nu)\delta(W^2 - M_R^2)$$

8 References

1. S.L. Adler et al., Princton. Annals of Physics: **50**, 189-311 (1968).

2. L.M. Sehgal et al., Technische Hochschure, Annals of Physics **133**, 79-153 (1981).
3. E.A. Paschos et al., Dortmund, Phys. Rev. D **69**, 014013 (2004).
4. E.A. Paschos et al., Dortmund, Phys. Rev. D **71**, 074003 (2005).
5. D.A. Norman, Tufts, MINERvA docDB-11371 August (2015).
6. S.J. Barish et al. (ANL), Phys. Rev. D **19**, 2521 (1979).
7. G.M. Radecky et al. (ANL), Phys. Rev. D **25**, 1161 (1982).
8. T. Kitagaki et al., Phys. BNL. Rev. D **34**, 2554 (1986).
9. H.J. Grabosch et al., Serpukhov. Z Phys. C **41**, 527 (1989).
10. G.T. Jones et al., CERN. Z. Phys C **43**, 327 (1989).
11. D. Allasia et al., CERN. Nucl. Phys. B **343**, 285 (1990).
12. A.A. Aguilar-Arevalo et al., MiniBooNE. Phys. Rev. D **83**, 052009 (2011).
13. Lancaster, Tom, and Stephen J Blundell. *Quantum Field Theory for the Gifted Amateur*. Oxford: Durham University, 2014.